14 Aug 2013

Development of Freeze-Form Extrusion Fabrication with Use of Sacrificial Material

Ming-Chuan Leu
Missouri University of Science and Technology, mleu@mst.edu

Diego A. Garcia

Recommended Citation

M. Leu and D. A. Garcia, "Development of Freeze-Form Extrusion Fabrication with Use of Sacrificial Material," *Proceedings of the 24th Annual International Solid Freeform Fabrication Symposium (2013, Austin, TX)*, pp. 326-345, University of Texas at Austin, Aug 2013.

DEVELOPMENT OF FREEZE-FORM EXTRUSION FABRICATION WITH USE OF SACRIFICIAL MATERIAL

Ming C. Leu and Diego A. Garcia

Department of Mechanical and Aerospace Engineering, Missouri University of Science and Technology, Rolla, MO 65409

Abstract

The development of Freeze-form Extrusion Fabrication (FEF) process to fabricate three-dimensional (3D) ceramic parts with use of sacrificial material to build support sections during the fabrication process is presented in this paper. FEF is an environmentally friendly, additive manufacturing process that builds 3D parts in a freezing environment layer-by-layer by computer controlled extrusion and deposition of aqueous colloidal pastes based on computer-aided design (CAD) models. Methyl cellulose was identified as the support material, and alumina was used as the main material in this study. After characterizing the dynamics of extruding alumina and methyl cellulose pastes, a general tracking controller was developed and applied to control the extrusion force in depositing both alumina and methyl cellulose pastes. The controller was able to reduce the time constant for the closed-loop system by more than 65% when compared to the open-loop control system. Freeze-drying was used to remove the water content after the part has been built. The support material was then removed in the binder burnout process. Finally, sintering was done to densify the ceramic part. The fabrication of a cube-shaped part with a square hole in each side that requires depositing the sacrificial material during the FEF process was demonstrated.

1. Introduction

Ceramic materials are applied widely in aerospace, automotive, biological, and other industries [1]. Many ceramic materials, such as Al_2O_3 and ZrB_2, can survive high temperatures (up to 2000°C for alumina and 3000°C for zirconium diboride), but processing these materials for use as 3D components is often challenging, expensive, and time-consuming. Building a ceramic part using additive manufacturing (AM) may reduce the material cost and build time for small runs and for parts with complex geometries.

Several AM processes can be used to produce ceramic parts. One is Fused Deposition of Ceramics (FDC) [2-5], which is based on the Fused Deposition Modeling (FDM) process invented by Scott Crump [6]. Stereolitography (SLA) [7,8], 3D Printing (3DP) [9], and Selective Laser Sintering (SLS) [10,11] are commercialized AM techniques for fabricating mostly polymer components, but with limited capabilities to make ceramic parts. Most existing paste extrusion based additive manufacturing systems utilize non-aqueous ceramic-based materials, and require a large amount of organizer binder for part fabrication (40-50 vol.%). Robocasting, which is an aqueous based extrusion freeform fabrication process, has been used to produce parts from different types of ceramics including oxides and non-oxides, and biomaterials [12]. However, it operates at room temperature, and has difficulty of preventing deformation (slumping) of large parts during the fabrication process.

One way to part deformation during the fabrication process is to freeze the paste rapidly after it is extruded and deposited. This can be accomplished by extruding aqueous-based pastes (with only a small amount of organic binder) at temperatures lower than the freezing point of the aqueous medium. Freezing during extrusion is the basis of the Freeze-form Extrusion Fabrication (FEF) process, which is a layer-by-layer deposition process that was developed at Missouri S&T by extending the technology of Rapid Freeze Prototyping (RFP) [13-15]. This environmentally friendly process has been developed and demonstrated for the freeform fabrication of 3D ceramic-based components. The aqueous paste used in the FEF process is extruded by a ram extruder, and the extruded material immediately deposits on a working surface (which may be a substrate or a previously deposited layer) that can be moved by an X-Y table. The surface temperature is set to a sub-zero temperature to freeze the material as it is deposited. The solids loading of the ceramic paste could be in the range of 45-55 vol.%.

The process parameters required to achieve better part quality in the FEF process have been studied previously [16-17]. Huang et al. [16] designed and implemented an on-off feedback controller to achieve more consistent material extrusion. This controller used the reading of extrusion force from a load cell to automatically adjust the ram velocity. Zhao et al. [17] found that due to effects such as air bubble release, agglomerate breakdown, and liquid phase migration, the ram velocity was difficult to control. Hence, an adaptive controller was designed and implemented to regulate the extrusion force.

The objective of the research as described in the present paper was to develop a method of fabricating ceramic parts that require the use of sacrificial material in the FEF process, which has not been investigated in the previous studies. Choosing a suitable support material for the process is challenging due to the need to prepare the paste in an aqueous-based solution with low binder content in order to keep the process environmentally friendly. For this purpose an existing single-extruder FEF machine was modified to a multiple-extruder machine capable of extruding multiple materials. By using one of these extruders to deposit the sacrificial material, which is removed during the post-processing, this FEF process with multiple extruders is capable of building parts with different types of features, e.g., internal holes and overhangs. After identifying methyl cellulose as a workable sacrificial material, mathematical models representing the dynamics of paste extrusion were developed through extrusion experiments with alumina and methyl cellulose pastes. For demonstration the fabricated green part was a cube-shaped part with a square hole in each side. The green part was shown to have good dimensional accuracy with respect to the CAD model. The green part was freeze-dried, debinded and sintered to remove the sacrificial material and achieve a high-density ceramic part.

2. Experimental Setup

The experimental setup for the freeze-form extrusion fabrication (FEF) process with multiple extruders consists of a motion subsystem, a real-time control subsystem, and extrusion devices. Figure 1 shows a phto of the overall system. The system consists of three linear axes (Parker Hannifin) each driven by a stepper motor (Empire Magnetics). The X, Y and Z axes each have 254 mm of travel range. The gantry motors each have a stepping angle of 1.8^{o}. Each motor has a resolver that measures the angular position and feeds the signal to a resolver-to-digital encoder converter module (RDE). The RDE converts the resolver signal to an equivalent encoder feedback signal, allowing the resolution of each axis at 2.5 μm per step. For each axis, the

maximum angular velocity is 50 rev/s, which provides a maximum velocity of 250 mm/s in linear movement. The maximum motor acceleration is 50 rev/s^2, which provides a maximum linear acceleration of 250 mm/s^2. The drives (National Instruments, NI) are used to amplify power from the two motion control cards for the stepper motors. Each card has outputs for up to four stepper motors plus inputs from encoders and limit switches for the four motors. The four outputs control the three stepper motors for the gantry axes and one stepper motor for an extruder. Another NI drive is used to regulate the other two extruder motors and to receive inputs from encoders and limit switches for two axes. The signals are amplified and then sent through a 32-pin connector to the two motion control cards. A National Instruments PXI 8176 real-time system with LabVIEW is used for software development and graphical user interface. The NI PXI-6025 multifunction data acquisition card is used for data input and output.

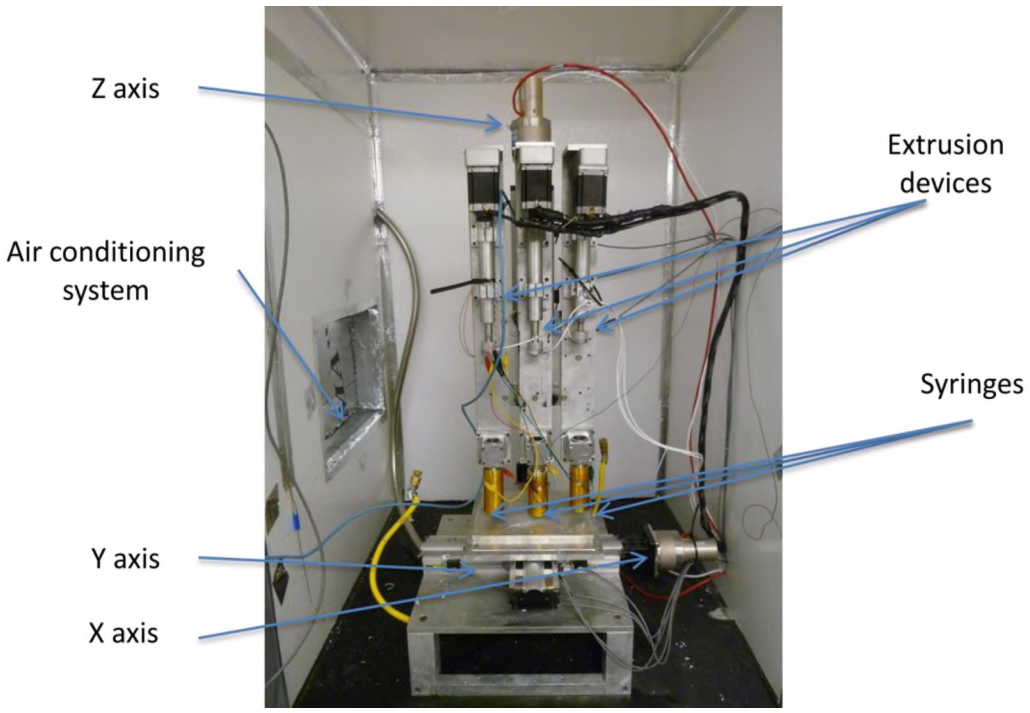

Figure 1. Experimental setup of the multiple-extruder FEF machine

Three extruders could be used for the deposition of three different pastes. They have the resolution of 2,846 steps/mm and could reach 72,882 steps/mm if using micro-stepping. The lead screw of each extruder had 20 cm of linear travel. Three 50 cm^3 syringes were used to contain the paste material for extrusion. A removable 580 μm diameter nozzle was used for depositing material. By adjusting the commanded speed of stepper motor, the material deposition rate and the force on the syringe for extrusion could be controlled. Three LC-301 load cells from Omega Engineering were mounted on the three extruder rams for extrusion force feedback. The load cell measured the extrusion force in the range of 0 to 2,250 N while the ram was applying pressure to the ceramic paste.

An air conditioning system was installed on the freezer box to maintain the work environment at sub-zero temperatures in the experimental setup. The syringes were mounted with heating cylinders to prevent the paste from freezing before exiting the nozzle during part fabrication. Two temperature controllers (Omega Engineering) were used to control the temperatures inside the box and in the heating cylinders. The temperature inside the box was normally set to -10 °C, and the temperature for the heating cylinders was set to 20 °C to result in 5 °C temperature at the nozzles.

Commercially available software, along with Matlab, was used with LabVIEW to coordinate the motion of the extruders and to switch between different materials during the fabrication process. Skeinforge, which is an open-source software package, was used to generate the tool path for both depositing both alumina and methyl cellulose pasts. The STL file of a CAD model is required to generate the tool path. The inputs to Skeinforge also include parameters such as extrudate width, stand-off distance, and table speed. The output of Skeinforge is tool path in G-code. A converter script in C++ was written to translate from G-code to an executable code by the FEF system.

3. Identification of Sacrificial Material

Two different materials were tested to determine the suitable sacrificial material for the FEF process. The first sacrificial material tested was carbon black, based on the previous research by Lewis et al. [18]. The composition of the carbon black paste used in our experiment was 48 vol.% carbon black ink, 4 vol.% methyl cellulose binder and 48 vol.% water. The carbon black paste did not work well due to viscosity inconsistency. The carbon black reacted differently at room temperature, which had ~30% humidity, than inside the freezer box at a sub-zero temperature, which had ~80% humidity. The high humidity inside the freezer box made the carbon black paste smudged after deposition. This phenomenon could be explained by the fact that the water content in the carbon black paste is increased by 4% when there is an increase of 10% in humidity in the environment [19]. Thus the carbon black paste viscosity was increased by almost 20 vol.% from its original composition due to increase of humidity from 30% to 80% when the paste was inside the freezer box. Carbon black was successfully used as a sacrificial material in the Direct Ink Writing (DIW) [18], which was performed at room temperature (without little humidity change) with the part fabricated in a pool of oil to prevent change of viscosity. However, it is not suitable for the FEF process because the FEF process is performed at a sub-zero temperature (with large humidity change).

Therefore, an alternative sacrificial material was investigated due to the incompatibility of carbon black for the FEF process. Methyl cellulose was identified as a favorable sacrificial material due to its good rheological properties at sub-zero temperatures. The methyl cellulose paste used in our study had 10 vol.% methyl cellulose and 90 vol.% water.

4. Modeling of Paste Extrusion Dynamics

The extrusion of two different aqueous pastes, alumina and methyl cellulose, was modeled by running extrusion tests to determine the values of parameters of a first-order system in the form of a transfer function. These values were determined from the system's response to a

reference input of ram velocity, with the extrusion force as the output. The transfer function between the extrusion force and the ram velocity is given by

$$\frac{F(s)}{V(s)} = \frac{K}{\tau s + 1} \tag{1}$$

where s is the Laplace operator, F is the extrusion force, V is the ram velocity, K is the extrusion process gain, and τ is the extrusion process time constant. The time constant for the first-order model for paste extrusion is calculated using the following equation

$$\tau = 2.2T_r \tag{2}$$

where T_r is the rise time (time taken from 10% to 90% of steady-state force). The gain is calculated using

$$K = \frac{F_{ss}}{V} \tag{3}$$

where F_{ss} is the steady-state force.

Table 1 shows the parameters calculated from the data collected from the experiment. It can be seen from this table that the time constant decreases as the ram velocity increases. By comparing the time constant of 22.15 s for the ram velocity of 0.1 mm/s and the time constant of 1.39 s for the ram velocity of 1 mm/s, we see that there is one order of magnitude difference in the time constant. The data from Table 1 was used to calculate the response of a first-order system using Equation (1). Figure 2 compares the simulation (using the calculated time constants) and experimental results, indicating that a first-order model is a good approximation of aluminum paste extrusion dynamics. From the values in Table 1, the relationship between the steady-state extrusion force vs. ram velocity is given in Figure 3, which shows a non-linear relationship between the steady-state force output and the ram velocity input. This relationship is attributed to a nonlinear relationship between the paste viscosity and the shear rate in a non-Newtonian fluid described by the Herschel –Bulkley model [20].

Table 1. Time constant, steady-state force, and gain for alumina paste extrusion at different ram velocity inputs

Velocity (mm/s)	T (s)	F_{ss} (N)	K (N/mm/s)
0.1	22.15	216.88	2168.8
0.2	7.20	280.10	1400.5
0.3	4.43	301.47	1004.9
0.5	3.20	340.27	680.54
0.7	1.76	363.21	518.87
1	1.39	405.25	405.25

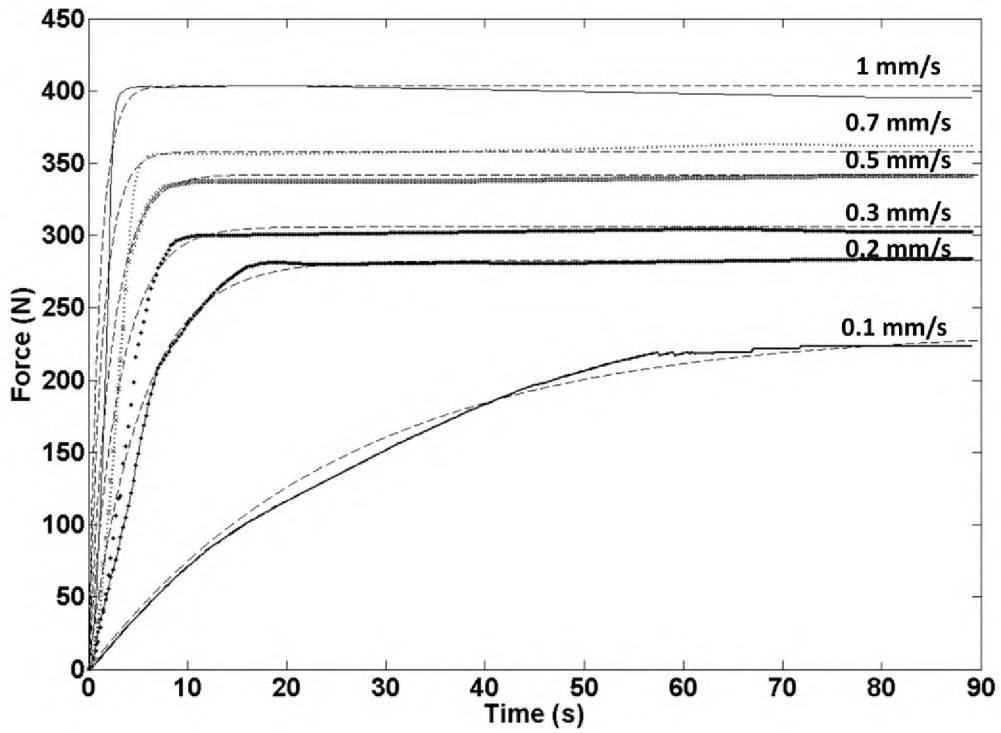

Figure 2. Comparison of simulation and experimental results based on gain and time constant for alumina paste extrusion from Table 1

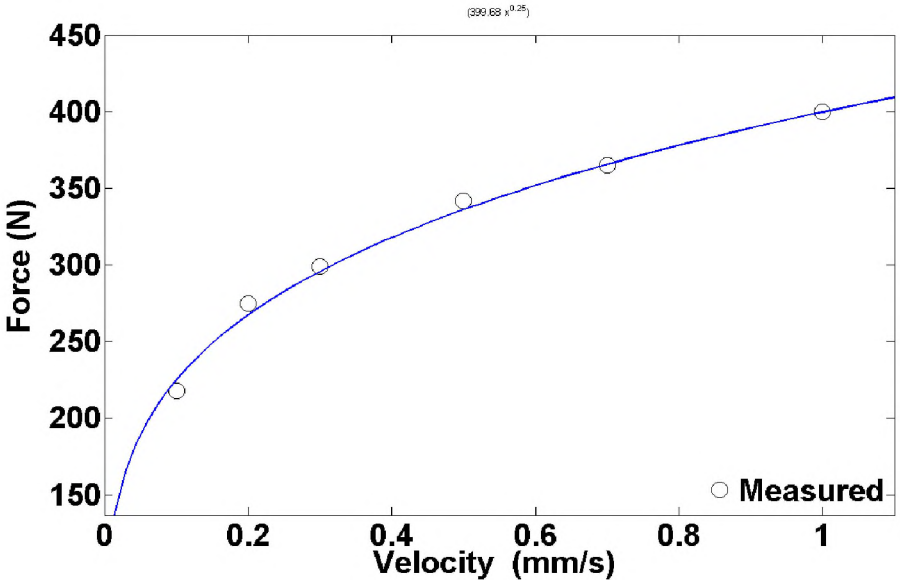

Figure 3. Relationship between steady-state force and ram velocity for alumina paste

Figure 4 shows the relationship between the time constant and the ram velocity for alumina paste extrusion using the parameter values in Table 1. The nonlinear relationship between time constant and ram velocity can be explained using the dynamic modeling of paste behavior by Li et al. [21,22], which considered some volume of air trapped inside the syringe and derived a dynamic extrusion force model to show that the time constant decreases when the extrusion force or ram velocity increases.

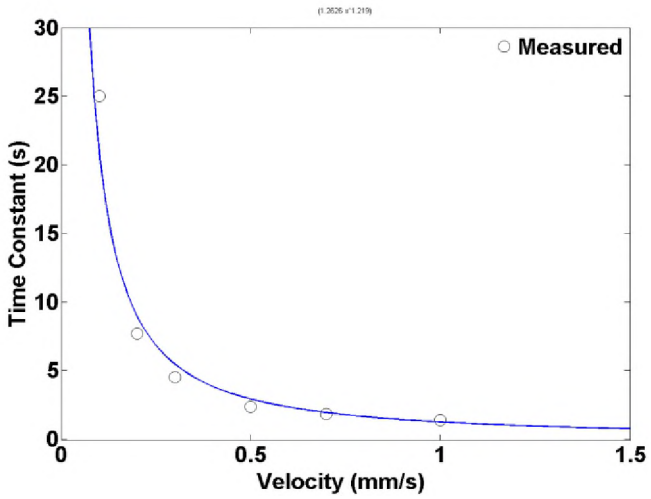

Figure 4. Relationship between time constant and ram velocity for alumina paste extrusion

In order to verify the values obtained in Table 1 and to apply a feedback force controller, the first-order model parameters were determined from another experiment where the ram velocity input was stepped alternately between 1 and -1 mm/s as shown in Figure 5. The time constant and system gain parameters were calculated in the digital domain using the Recursive Least Square method (RLS). A first-order dynamic model describing the paste extrusion force of the process in the digital domain is

$$G(z)=\frac{F(z)}{V(z)}=\frac{b}{z+a}=\frac{K(1+a)}{z+a} \tag{4}$$

where z is the forward shift operator, F is the extrusion force (N), V is the command velocity (mm/s), and K is the unknown model gain (N/mm/s).

The time constant and gain, respectively, are

$$\tau=-\frac{T}{ln(-a)} \tag{5}$$

$$K=\frac{b}{1+a} \tag{6}$$

where T is the sampling time, and τ is the time constant.

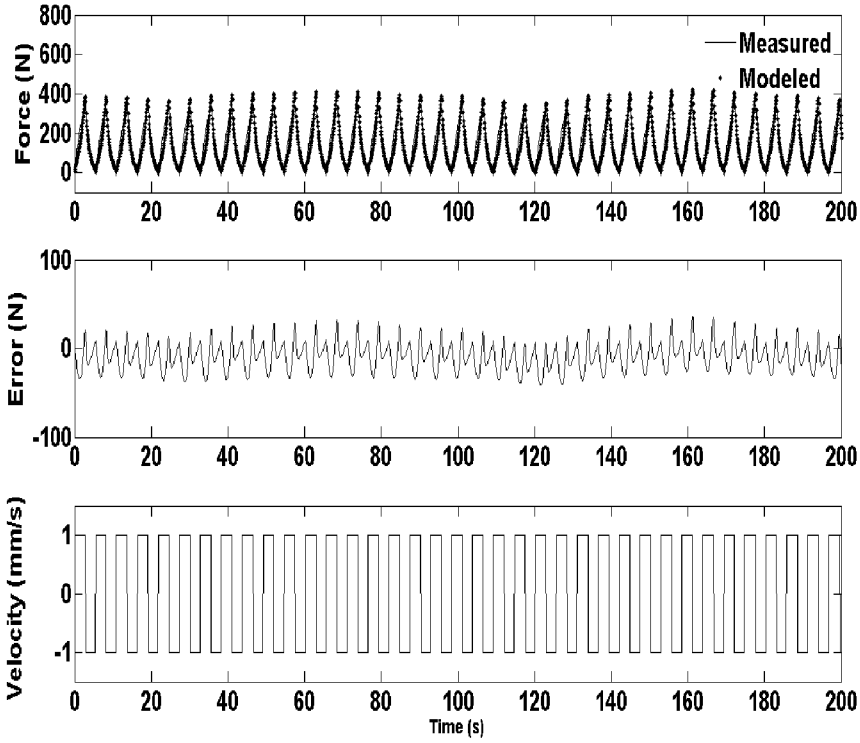

Figure 5. Comparison of modeled and measured results with a step reference input alternating between 1 and -1 mm/s for extrusion of alumina paste

The extrusion of methyl cellulose paste also exhibits a first-order behavior between the extrusion force output and the input ram velocity. Based on the obtained force-velocity data, the time constant and steady-state force were calculated and given in Table 2. Like the extrusion of alumina paste, the time constant decreases with increase in ram velocity in the extrusion of methyl cellulose paste.

Table 2. Time constant, steady-state force, and gain for methyl cellulose paste at different ram velocity inputs

Velocity (mm/s)	T (s)	F_{ss} (N)	K (N/mm/s)
0.1	18.55	176.23	1762.3
0.2	6.10	222.14	1110.7
0.3	3.44	248.37	827.9
0.5	2.90	296.24	592.48
0.7	1.75	320.54	457.14
1	1.36	353.20	353.20

5. Controller Design and Implementation

Due to certain effects of extrusion such as the release of air bubbles, breakdown of agglomerates, and change in paste properties as a result of liquid phase migration, the extrusion force is difficult to control in an open loop [16-17]. Thus a General Tracking Controller (GTC) was implemented in this study to regulate the extrusion force in a close-loop manner and to allow extrusion on demand in the FEF process. The objectives of the closed-loop controller are to extrude the paste at a constant rate, to coordinate the start of extrusion with the gantry motion, and to reject disturbances with desired error dynamics. The block diagram of a GTC controller is depicted in Figure 6.

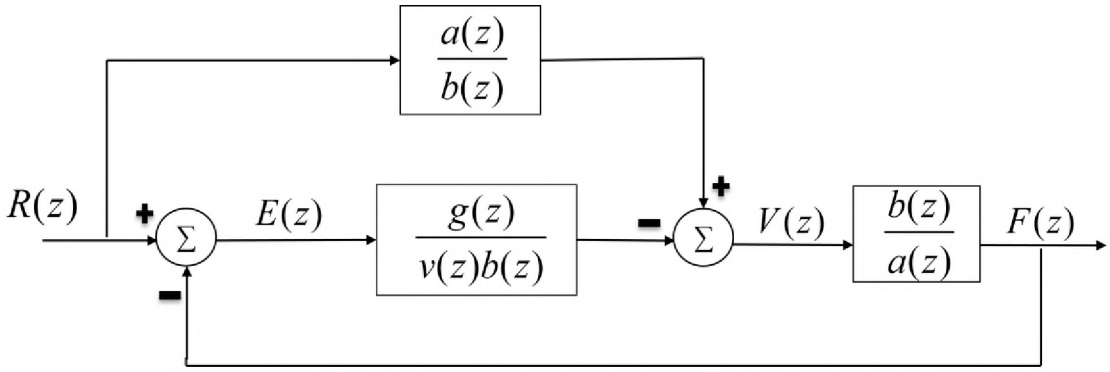

Figure 6. Block diagram of the general tracking controller

The control signal is related to error and reference signals by

$$b(z)v(z)V(z) = v(z)a(z)R(z) + g(z)E(z) \tag{7}$$

where $v(z)a(z)$ is the disturbance-generating polynomial, and $v(z) = z - 1$ is the reference disturbance for a step input. Because $b(z)V(z) = a(z)F(z)$ and $E(z)$ is the error defined by

$$E(z) = R(z) - F(z) \tag{8}$$

we have

$$[v(z)a(z) - g(z)]E(z) = 0 \tag{9}$$

where $R(z)$ is the reference ram extrusion force, $F(z)$ is the measurement from the load cell, $a(z)$ is the denominator of the open-loop transfer function, and $g(z)$ is a first-order polynomial

$$g(z) = g_1 z - g_0 \tag{10}$$

and g_1 and g_0 are determined by the desired closed-loop error dynamics using the following equations:

$$g_1(z) = -1 + a\ - \alpha_1 \tag{11}$$

$$g_0 = -a - \alpha_0 \tag{12}$$

where

$$\alpha_1 = -e^{(-T/\tau_1)} \tag{13}$$

and

$$\alpha_0 = -e^{(-T/\tau_2)} \tag{14}$$

The closed-loop characteristic equation is

$$\alpha(z) = z^2 + \alpha_1 z + \alpha_0 \tag{15}$$

Equation (9) can be rewritten as

$$[z^2 + (1 - a - g_1)z + (-a - g_0)]E(z) = 0 \tag{16}$$

For the second-order system to have a response similar to a first-order system, one pole should have a much smaller magnitude than the other pole. We achieved this by making the second pole at least one order of magnitude smaller than the dominant pole, and shortening the settling time as much as possible without causing system instability with the dominant pole.

A general tracking controller as described above was implemented for control of alumina paste extrusion. Using Equations (11) – (14) and the model parameters calculated with the RLS method, the obtained parameters were g_1 = -1.07 and g_0 = 1.06. To validate the working of the GTC, an input square signal was given with low and high limits of 100 N and 400 N, respectively, as shown in Figure 7. Two over-damped poles were selected with the time constants τ_1= 0.5 s and τ_2= 0.05 s, thus the time constant of the closed-loop system was determined by τ_1. The time constant τ_1 was determined by the mechanical limitations of the FEF system. The maximum input velocity for the alumina paste extrusion process in the FEF system was 2 mm/s, at which the maximum force of 550 N provided by the stepper motor in the system was reached. The open-loop time constant for 2 mm/s ram velocity input was calculated using Equation (4) and the time constant obtained was τ = 0.48 s . The closed-loop time constant was chosen as 0.5 s, in order to have the quickest response of the system without overloading the motor. The reference force for extrusion of alumina paste was set at 400 N, which is slightly less than 550 N for margin of safety. The force of 100 N was used to stop extrusion based on experimental test runs. The GTC tracked the reference force with an error of +/-10 N, indicating a consistent extrusion rate. From Figure 8, the time constant of the closed-loop system calculated from the rise time is approximately 0.5 s using Equation (2). This time constant is reduced by 65% from 1.39 s (Table 1) in the open-loop system for a 400 N output force (or 1 mm/s in ram velocity). For a smaller extrusion force (or ram velocity), the percentage reduction in the time constant is larger because the time constant in the closed-loop system remains unchanged while the time constant in the open-loop system increases with decrease in extrusion force (or ram velocity) as seen in Table 1. The ram input velocity was set to +/- 2mm/s in order to have a faster response of the system without getting into instability. Higher velocities would cause the stepper motor to skip and not able to track the reference force as desired.

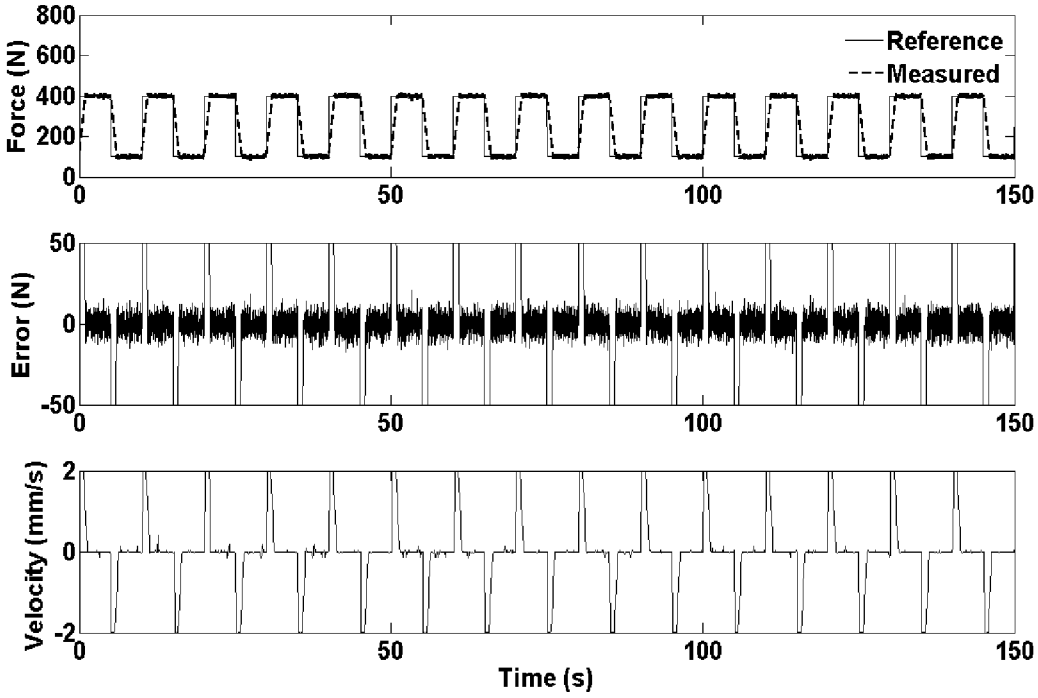

Figure 7. Response of the general tracking controller for a reference ram force input for extrusion of alumina paste

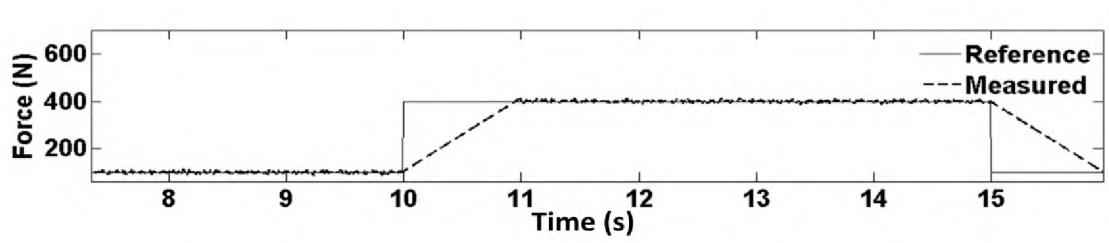

Figure 8. Reference vs. measured force using the GTC with a rise time of 1s for extrusion of alumina paste

A series of tests was conducted to find a relationship between the extrudate velocity and the reference extrusion force in the close-loop system. Table 3 was generated by varying the reference force from 150 N to 200 N, then to 300 N, and finally to 400 N. The nozzle tip was positioned along the Z direction 50 mm above the X-Y table in the gantry system. The extrudate velocity was calculated by measuring the time it took for the paste to reach the X-Y table from the moment it was extruded from the tip. A stopwatch with a resolution of 0.1 s was used for this time measurement. Six test runs per reference force were conducted and the measured data were averaged. The different tests per reference force show similar values, verifying the advantage of using the GTC for consistent paste extrusion.

Table 3. Relationship between reference extrusion force and extrudate velocity for alumina paste

Test run	Distance (mm)	Force (N)	Test 1 (s)	Test 2 (s)	Test 3 (s)	Test 4 (s)	Test 5 (s)	Test 6 (s)	Mean extrudate speed (mm/s)
1	50	150	80.1	82.3	85.4	84.3	82.1	82.8	0.6
2	50	200	42.1	40.1	44.2	43.2	42.1	42.3	1.18
3	50	300	20.1	21.2	22.0	21.8	20.9	21.2	2.35
4	50	400	12.3	13.1	14.2	13.5	12.9	13.2	3.78

The relationship between extrusion force and extrudate velocity in Table 3 is plotted in Figure 9. The *y* intercept in this figure shows that when the extrudate velocity is zero, the steady-state force is 106.6 N, indicating that the minimum force required to extrude the alumina paste from the nozzle tip is slightly larger than 100 N. If the extrusion force is less than this threshold, extrusion of the paste will cease because the applied ram force is not sufficient to overcome the shear stress required for the paste flow.

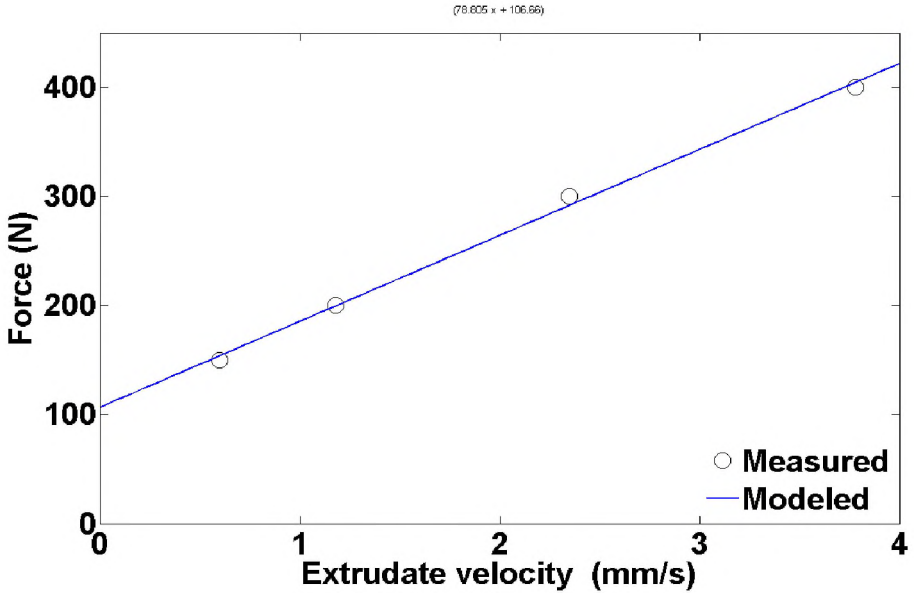

Figure 9. Reference force extrusion vs. extrudate velocity for alumina paste

For extrusion of methyl cellulose paste, a general tracking controller was also implemented. A series of tests was conducted to find the relationship between the extrudate velocity and the reference force in the closed-loop system for extrusion of methyl cellulose paste. Based on experimental test runs, the reference force of 350 N was used to start the paste extrusion and the reference value of 50 N was used to stop the extrusion. The closed-loop time constant was calculated based on the open-loop time constant for a ram velocity of 2 mm/s. The time constant of 0.5 s was again chosen, which is the same as the time constant used in the

closed-loop control of alumina paste extrusion. With this time constant the rise time was approximately 1 s, and thus the time constant of the open-loop system (1.36 s) was reduced to 0.5 s (65% reduction) for the steady-state extrusion force of 350 N in the closed-loop system. The time constant of the closed-loop system was approximately 0.5 s as expected. The small time constant and force error result in a consistent extrusion rate when depositing methyl cellulose paste during part fabrication.

6. Effects of Process Parameters

The quality of part fabricated by the FEF process is affected by parameters including the stand-off distance and table speed. This section discusses the determination of effective parameter values for the FEF process with the use of sacrificial material. In all of the experiments, the diameter of the needle nozzle was 580 μm.

By using the maximum extrusion force in the FEF process, which was 400 N for alumina and 350 N for methyl cellulose, the extrudate diameter was determined experimentally as 780 μm and 760 μm, respectively, for a freezer temperature of -10 °C. Experiments were conducted to measure the extrudate width by varying the stand-off distance. The range of stand-off distance varied from 700 μm to 400 μm in decrements of 100 μm in the experiments. The path was a serpentine trajectory of 4 lines and the table speed was 8 mm/s. The lines were measured using a caliper with a resolution of 10 μm. Five lines were deposited for each stand-off distance in order to see the repeatability of the process in having a consistent extrudate width. It was observed that the shorter the stand-off distance, the wider the extrudate line. Note that the extrudate diameter of the paste coming out of the nozzle had a diameter larger than the stand-off distance. This caused the extrudate line to flatten out, resulting in an approximately rectangular (instead of circular) cross-sectional area. The extrudate widths at different stand-off distances for alumina paste extrusion are given in Table 4. The same experiment was repeated for methyl cellulose paste.

Table 4. Relationship between stand-off distance and extrudate width for alumina paste

Test run	Stand-off distance (μm)	Line 1 Width (mm)	Line 2 Width (mm)	Line 3 Width (mm)	Line 4 Width (mm)	Line 5 Width (mm)	Mean Width (mm)
1	400	1.23	1.25	1.22	1.21	1.23	1.22
2	500	1.15	1.12	1.10	1.11	1.11	1.11
3	600	1.0	0.98	0.96	0.95	0.94	0.96
4	700	0.80	0.79	0.81	0.80	0.76	0.79

The cross sections from rectangular blocks fabricated at different stand-off distances are shown in Figure 10. The block with 600 µm stand-off distance (Figure 10a) shows extrudate lines with rounder edges and some holes between the extrudate lines. The blocks built at 500 µm and 400 µm stand-off distances (Figure 10b & 10c) show extrudate lines with sharper edges and also fewer and smaller holes between the extrudate lines. Therefore, 400 µm and 500 µm are more desirable stand-off distances. In further experiments the stand-off distance of 500 µm was used in extruding both alumina and methyl cellulose pastes.

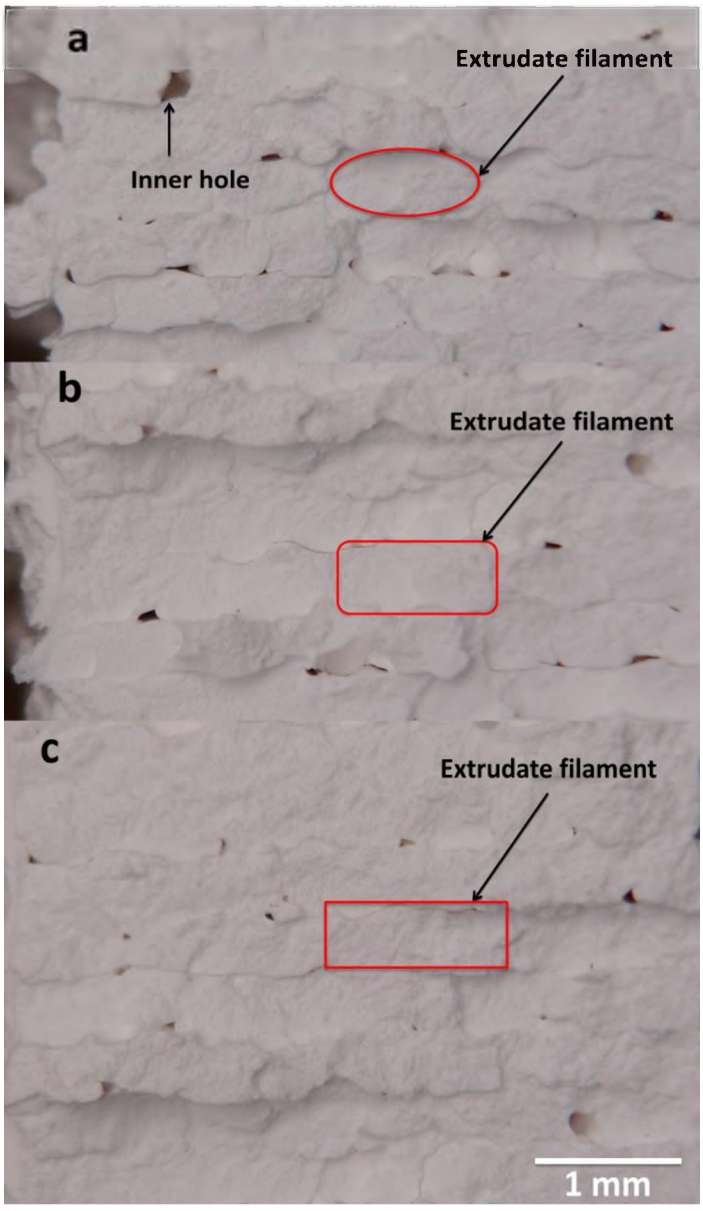

Figure 10. Cross sections of extrudate blocks with the stand-off distance of (a) 600 µm, (b) 500 µm, and (c) 400 µm

The table speed is crucial to the quality paste deposition. Six test runs were conducted in which the table speed was varied from 4 mm/s to 14 mm/s in increments of 2 mm/s, while the extrudate speed was 4 mm/s. Figure 11 and shows the results of extrusion using an extrusion force of 400 N for alumina paste and 350 N for methyl cellulose paste (at 500 µm stand-off distance). It can be seen that when the table speed was 8 mm/s, the deposition of both alumina and methyl cellulose pastes had relatively uniform width compared with the other table speeds. At velocities higher than 10 mm/s, inconsistency in the width of extrudate line was observed. Such a deposition could lead to gaps between lines during the rastering process, resulting in poor-quality parts. It was reported previously that maintaining the extrusion speed at the table speed is advisable [16]. However, having the table speed same as the extrudate speed could possibly result in an over-extrusion of paste surrounding the nozzle tip due to the stand-off distance less than the extrudate diameter, if the nozzle wall is not thick enough.

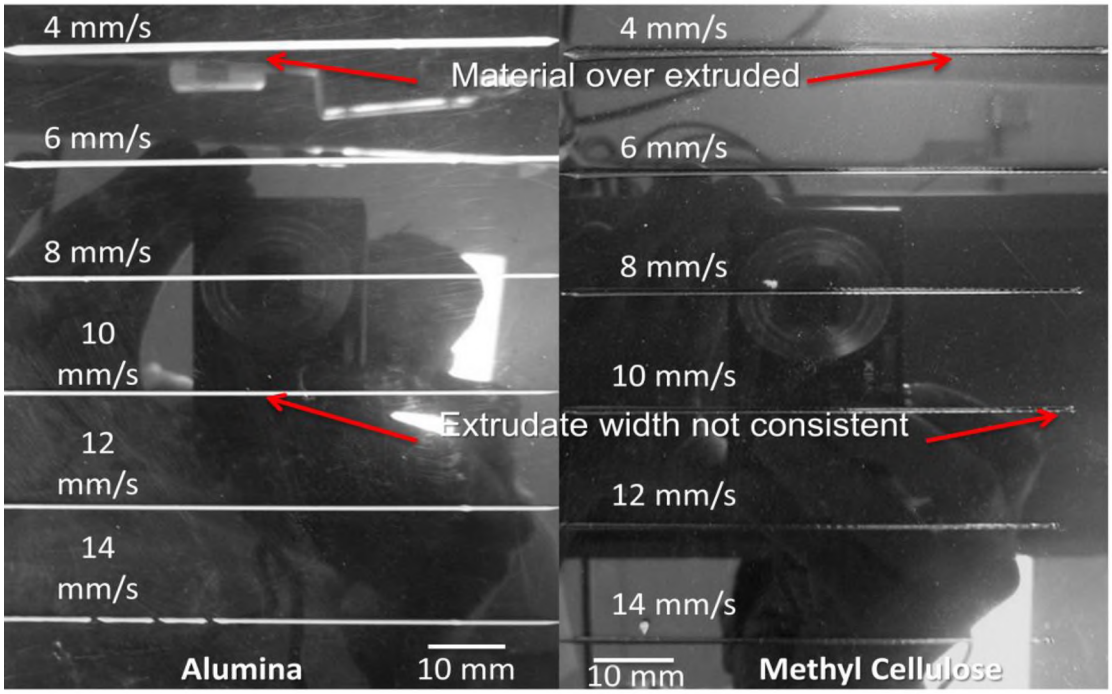

Figure 11. Different table speeds for extrusion of alumina paste (left) at 400 N extrusion force and for extrusion of methyl cellulose paste (right) at 350 N extrusion force

The equation based on conservation of paste flow is

$$V_T = \frac{V_{ex}\pi D^2}{4wh} \tag{17}$$

where V_T is the Table speed, V_{ex} is the extrudate speed, D is the extrudate diameter (780 µm for alumina), w is the extrudate width, and h is the stand-off distance. From Equation (17) it can be calculated that when the table speed is 4 mm/s, the extrudate width is 1.91 mm. This is much larger than the outer diameter of the nozzle, thus at this speed there was an over-extrusion of

paste material and the width of the extruded paste line was not very uniform in Fig. 11. When the table speed is 6 mm/s, the line width of the extruded paste is 1.21 mm, which is slightly larger than the nozzle's outer diameter. When the table speed is 8 mm/s, the extruded paste line width is 0.95 mm, which is slightly smaller than the nozzle's outer diameter. The above explains why the extrudate line is most uniform in Fig. 11 when the table speed is 8 mm/s.

7. Part Fabrication Results and Discussion

Several parts were fabricated to demonstrate the capabilities of the developed FEF system. The freezer temperature was -10 °C, and the stand-off distance used was 500 µm. For purpose of improving part quality, there was a waiting time of 10 s between layers. Figure 12 shows the CAD model for a cube with square through holes in all sides and an alumina part fabricated by the FEF process with use of sacrificial material for the CAD model.

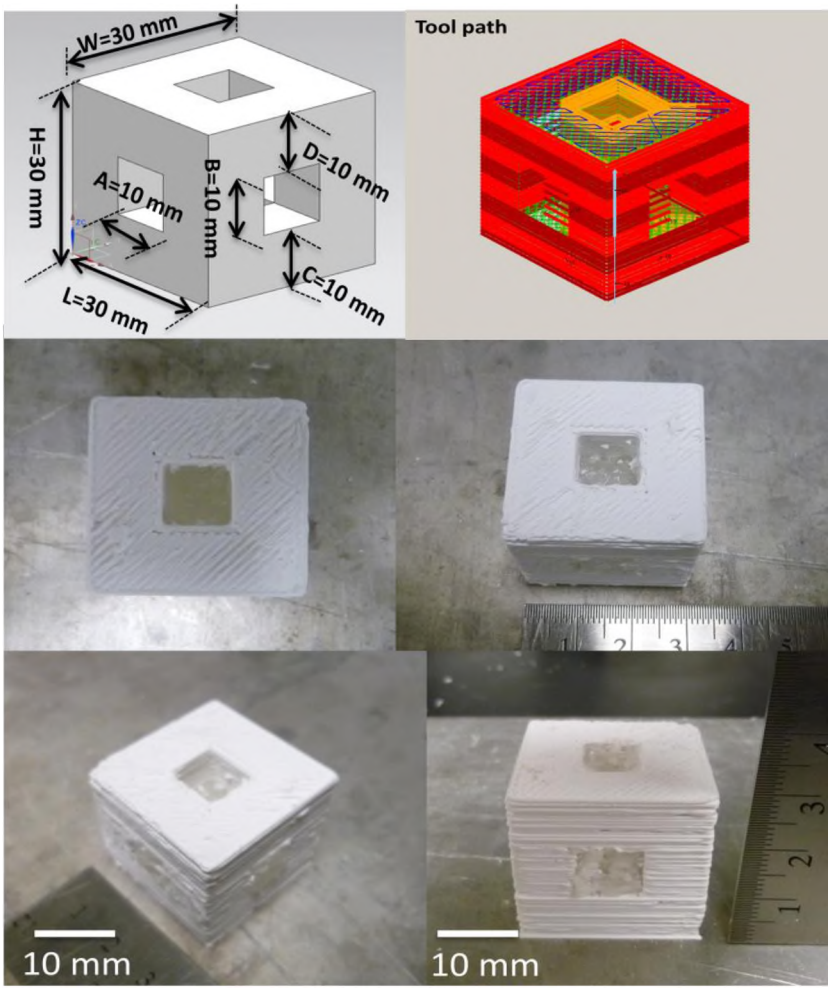

Figure 12. CAD model of a cube with a square hole on each side and the extruded part with sacrificial material

The sacrificial material methyl cellulose was burnt out to remove it from the part prior to sintering. Then sintering was performed to densify the alumina part into a solid ceramic structure. The binder burnout process began slowly with a ramp of 2 °C/min and continued until reaching 400 °C. After the methyl cellulose was burned out, the slope of ramp was increased to a rate of 10° C/min until 1550 °C. After reaching 1550 °C, the temperature was kept constant for one hour to sinter the part. Then the furnace was cooled down at a ramp of 75 °C/min until reaching room temperature. The slow ramp rate of 2 °C/min to 400 °C was based on previous experiments in burning out organics from ceramic bodies [16]. The critical temperatures in the binder removal and part sintering were obtained using Thermogravimetric Analysis (TGA) to measure the weight loss of material as a function of temperature.

Dimensional measurements were taken from the green parts using a caliper with a resolution of 1 μm. The cube and mushroom parts were selected because their dimensions could be measured easily with a caliper. In Figure 12, each measured dimension is labelled with a letter. Four measurements were taken from random locations from the green part. The measured data together with the means and standard deviations are given in Table 5. From this table, the dimensions of the green part for the cube varied between 0.1% to 3.0% compared with the dimensions of the CAD model. The differences were small and would suggest good accuracy of part fabricated by the FEF process.

Table 5. Measurements for a cube-shaped part in its green state

Measurement	L(mm)	W(mm)	H(mm)	A(mm)	B(mm)	C(mm)	D(mm)
CAD model	30	30	30	10	10	10	10
1	30.20	30.10	30.17	10.10	10.20	10.6	11.0
2	29.81	29.88	29.87	9.90	9.60	0.97	9.80
3	29.75	30.40	30.23	9.80	9.80	0.90	9.20
4	30.40	29.95	29.80	11.00	1.10	0.96	9.90
Mean	30.04	30.08	30.01	10.20	10.10	9.70	9.90
Difference	0.04	0.08	0.1	0.20	0.10	0.30	0.10
% Error	0.10	0.20	0.30	2.0	1.0	3.0	1.0
Standard Deviation	0.31	0.23	0.21	0.05	0.61	0.60	0.70

After sintering, eight measurements were taken from different points for each dimension for the cube-shaped part. Table 6 gives the measured data together with means and standard deviations for the sintered part. This table shows that the standard deviation varied between 0.7% and 1%, and that the percentage of shrinkage for the various dimensions was in the range of 16-23% compared to the green part after sintering.

Table 6. Measurements for the cube-shaped part after sintering

Test	L (mm)	W (mm)	H (mm)	A (mm)	B (mm)	C (mm)	D (mm)
1	25.19	25.11	25.09	7.96	7.74	7.87	7.77
2	25.09	25.07	24.88	7.90	7.65	7.80	7.70
3	24.92	25.02	25.12	7.84	7.82	7.74	7.82
4	25.30	24.87	24.97	8.04	7.80	7.90	7.86
5	25.15	24.92	25.00	7.84	7.82	7.92	7.84
6	25.07	24.87	24.77	7.94	7.76	7.88	7.92
7	24.96	25.13	25.06	7.90	7.90	7.79	7.84
8	25.82	25.08	24.80	8.00	7.82	7.91	7.78
Mean	25.18	25.00	24.96	7.92	7.78	7.85	7.81
Standard deviation	0.28	0.10	0.13	0.071	0.073	0.06	0.06
% Shrinkage	16	17	17	22	23	19	21

It should be noted that part accuracy can be improved by using nozzles of smaller diameters. For example, a nozzle of 300 μm in diameter can be used in lieu of the nozzle of 580 μm used in the current FEF process. However, using a smaller nozzle will increase the part build time. To decrease the building time, the extrusion force can be increased in order to increase the extrudate velocity. However, since the extrusion force is limited by the motor power, more powerful motors will be needed in order to increase the extrusion force.

8. Conclusions

A freeze-form extrusion fabrication (FEF) system with multiple extruders operating in a freezing environment (about -10 °C) has been developed and successfully implemented. The parts were built by extruding and depositing aqueous alumina paste as the main material, and methyl cellulose was identified as the sacrificial material. An empirical first-order model was used to represent the extrusion dynamics for both alumina and methyl cellulose pastes, with the ram velocity as the input and extrusion force as the output. A general tracking controller was applied to control the extrusion force. The controller reduced the time constant for the closed-loop system by 65% and more when compared to the open-loop control system in extrusion of both alumina and methyl cellulose pastes. The capability of the developed system was demonstrated by fabricating a cube-shaped part with square holes on all sides. The dimensional accuracy of the green part was in the range of 0.1 – 3.0% compared to the CAD model. The sacrificial material was removed successfully during the binder burnout. Shrinkage varied between 16% and 23% for the various dimensions of the part after sintering.

Acknowledgements

This project was funded by NSF grant #CMMI-0856419 with matching support from the Boeing company through the Center for Aerospace Manufacturing Technologies at the Missouri University of Science and Technology.

References

[1] "Advanced Ceramics Technology Roadmap-Charting Our Course," Sponsored by U.S. Advanced Ceramic Association and U.S Department of Energy, Prepared by Energetics, Inc. and Richerson and Associates, December 2000.

[2] S. Rangarajan, Q. Qi, N. Venkataraman, A. Safari, and S. C. Danforth, "Powder Processing, Rheology, and Mechanical Properties of Feedstock for Fused Deposition of Si3N4 Ceramics," *Journal of the American Ceramic Society*, *83*(7), pp. 1663-1669, 2000.

[3] A. Bandyopadhyay, P. Panda, M. Agarwala, S. Danforth, and A. Safari, "Processing of Piezocomposites by Fused Deposition Technique," *Journal of the American Ceramic Society, 80*(6), pp. 1366-1372, 2000.

[4] G. M. Lous, I. A. Cornejo, T. F. McNlty, A. Safari, and S. C Danforth, "Fabrication of Piezoelectric Ceramic/Polymer Composite Transducers Using Fused Deposition of Ceramics," *Journal of the American Ceramic Society, 83*(1), pp. 124-28, 2000.

[5] A. Bandyopadhayay, R. K.Panda, V. F. Janas, M. K Agarwala, S. C. Danforth, and A. Safari, "Processing of Piezocomposites by Fused Deposition Technique," *Journal of the American Ceramic Society*, *80*(6), pp. 1366-72, 1997.

[6] S. Crump, Apparatus and Method for Ceramic Three-Dimensional Objects, U.S. Patent No. 5121329, 1992.

[7] P. F. Jacobs, *Rapid Prototyping & Manufacturing: Fundamentals of Stereolithography*, SME publication, Dearborn, MI, 1992.

[8] M. L. Griffith and J. W. Halloran, "Freeform Fabrication of Ceramics via Stereolithography," *Journal of the American Ceramic Society, 79*(10), pp. 2601–2608, 1996.

[9] M. E. Sachs, J. S. Haggerty, M. J. Cima, and P. A. Williams, "Three Dimensional Printing Techniques," U.S. Patent No. 5204055, 1993.

[10] J. J. Beaman, J. W. Barlow, D. L. Bourell, J. W. Barlow, R. H. Crawford, and K. P. McAlea, *Solid Freeform Fabrication: A New Direction in Manufacturing*, Kluwer Academic Publishers, 1997.

[11] M. C. Leu, S. Pattnaik, and G. E. Hilmas, "Investigation of Laser Sintering for Freeform Fabrication of Zirconium Diboride Parts," Journal of Virtual and Physical Prototyping, 7(1), pp. 25-36, 2012.

[12] J. Cesarano III, R. Segalmen, and P. Calvert, P., "Robocasting Provides Moldless Fabrication from Slurry Deposition," *Ceramics Industry*, 148, pp. 94-102, 1998.

[13] M. C. Leu, Q. Liu, and F. D. Bryant, "Study of Part Geometric Features and Support Materials in Rapid Freeze Prototyping," *Annals of the CIRP, 52*(1), pp. 185-188, 2003.

[14] M. C. Leu, Q. Liu, and F. D. Bryant, "Study of Part Geometric Features and Support Materials in Rapid Freeze Prototyping," *Annals of the CIRP, 52*(1), pp. 185-188, 2003.

[15] G. Sui and M. C. Leu, "Investigation of Layer Thickness and Surface Roughness in Rapid Freeze Prototyping," *ASME Journal of Manufacturing Science Engineering*, pp. 20-61, 2007.

[16] T. Huang, M. S. Mason, X. Zhao, G. E. Hilmas, and M. C. Leu, "Aqueous-based Freeze-form Extrusion Fabrication of Alumina Components," *Rapid Prototyping Journal*, *15*(2), pp. 88 – 95, 2009.

[17] X. Zhao, R. G. Landers, and M.C. Leu, "Adaptive-Control of Freeze-form Extrusion Fabrication Process," *ASME Journal of Manufacturing Science Engineering*, pp. 20-61, 2007.

[18] J. A. Lewis, J. A. Smay, J. Stuecker, and J. Cesarano III, "Direct Ink Writing of Three-Dimensional Structures," *Journal of the American Ceramic Society, 89*(12), pp. 3599-3609, 2006.

[19] C. S. Dewey, P. K. Lefforge, and G. L. Cabot, "Moisture Sorption by Carbon Black," *Industrial and Engineering Chemistry*, pp 1045-1050, 1932.

[20] Herschel, W. H and Bulkley, R., "Consistency of Measurements in Rubber-Benzene Solutions," *Colloid Journal 39*, pp. 291-300,1926.

[21] M. Li, L. Tang, L., R. G. Landers and M. C. Leu, "Extrusion Process Modeling for Aqueous–based Ceramic Pastes, Part 1: Constitutive Model," ASME Journal of Manufacturing Science and Engineering, 2013 (in press).

[22] M. Li, L. Tang, L., R. G. Landers and M. C. Leu, "Extrusion Process Modeling for Aqueous–based Ceramic Pastes, Part 2: Experimental Verification," ASME Journal of Manufacturing Science and Engineering, 2013 (in press).